Atomistic Simulation of Slow Grain Boundary Motion

Chuang Deng and Christopher A. Schuh*

*Department of Materials Science and Engineering, Massachusetts Institute of Technology, 77 Massachusetts Avenue,
Cambridge, Massachusetts 02139, USA*

Existing atomistic simulation techniques to study grain boundary motion are usually limited to either
high velocities or temperatures and are difficult to compare to realistic experimental conditions. Here we
introduce an adapted simulation method that can access boundary velocities in the experimental range and
extract mobilities in the zero driving force limit at temperatures as low as $\sim 0.2 T_m$ (T_m is the melting
point). The method reveals three mechanistic regimes of boundary mobility at zero net velocity depending
on the system temperature.

Grain boundary (GB) motion during, e.g., grain growth
or recrystallization, governs the kinetics of microstructure
formation and evolution in every class of polycrystalline
materials. Because controlled experiments on GB motion
are difficult to perform and require large investments of
time to prepare and then test specimens [1], there has been
a large and rising interest in the use of atomistic simula-
tions, such as molecular dynamics (MD), to rapidly and
accurately extract the fundamental parameters characteriz-
ing boundary motion [2–14]. MD techniques developed to
study GB motion in recent years can be grouped into two
categories. First, the "driven motion" methods seek to
drive the GB under a controlled driving force and measure
the velocity of GB migration [4,7–9,12–14]. In contrast,
the "fluctuating boundary" techniques are based on char-
acterizing the fluctuations of an interface during exposure
to high temperatures, in the limit of zero net velocity
[10,11]. Both of these technique classes have provided
insights on the mechanisms and kinetics of boundary mo-
tion, but they are significantly limited by the short time
scale inherited from the MD method itself. Driven motion
methods generally access velocities several orders of
magnitude higher than are usually obtained from experi-
ments [1,4,7,8], and also seem to activate different mecha-
nisms with very low activation energies compared to
experiments [4,7]. Similarly, the fluctuating boundary
methods require very high temperatures, usually above
about $0.80 T_m$ (T_m is the melting point) [10,11], in order
to obtain measurable interface fluctuations over the MD
time scale.

Our purpose in this Letter is to propose a new, hybrid
simulation method that improves the range of accessible
time scales for GB motion simulations, without need of
vastly greater computing power. Our approach involves
two key contributions: first, we discuss a method of en-
hancing the statistics of GB motion simulations, and sec-
ond, we present a hybridization of the "driven motion" and
"fluctuating boundary" methods to simulate slow bound-
ary motion under small biases. We report the simulation of

GB motion at velocities in the experimental range, and
extract boundary mobilities at temperatures as low as
$\sim 0.2 T_m$.

We use MD with embedded-atom method (EAM) poten-
tials to study several GBs, including a $\Sigma 7$ symmetric tilt
boundary in Al, a $\Sigma 5$ symmetric tilt boundary in Ni, and a
$\Sigma 3$ coherent twin boundary in Ni. The geometry of the
computational cell and details of the MD procedures can
be found in the supplemental materials [15]. Figure 1(a)
shows an example of the computational cell for an Al $\Sigma 7$
GB at 750 K ($\sim 0.8 T_m$), with the boundary identified by the
non-fcc coordinated atoms and characterized by significant
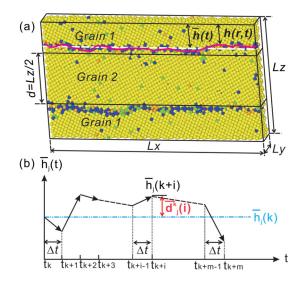shape fluctuations. In Fig. 1(a), the solid line tracks the local

FIG. 1 (color online).   (a) Schematic and atomistic configura-
tion of the computational cell for an Al $\Sigma 7$ GB at 750 K, with
atoms colored according to local crystal structure. The simula-
tion cell dimensions {Lx, Ly, Lz} are {15.8, 1.4, 18.3} nm.
(b) Schematic showing the definition of GB displacement $\bar{d}(i)$
during time interval $i \cdot \Delta t$ relative to an arbitrary position $\bar{h}(k)$
at $t = t_k$.

position of the upper GB, while the dashed line marks its average position along the z direction.

In order to study the mobility and motion of GBs in this computational cell, we adapt the interface-random-walk method described in Ref. [10]. This method takes advantage of the fact that, statistically, at a given temperature the average GB position among a large number (N) of independent GBs of identical geometry but different initial conditions should remain unchanged, while the variance of GB position should increase linearly with time [10]:

$$D = \frac{d\langle \bar{d}^2 \rangle}{dt} \sim \frac{2MkT}{A}, \qquad (1)$$

where D is the diffusion coefficient, t is time, T is temperature, A is the interface area, $\langle \bar{d}^2 \rangle$ is the mean square GB displacement, and M is the GB mobility, which follows an Arrhenius relation with an activation energy Q_m.

In the original interface-random-walk method as developed in Ref. [10], a number l of independent simulations were conducted to extract $N = 2l$ data points [two boundaries per simulated cell, Fig. 1(a)], from which the variance was computed. In order to increase the precision of this technique, we inflate the effective sample size N by several orders of magnitude, not by performing more simulations, but by recognizing that each simulation comprises many sampling opportunities of shorter duration, based on the arbitrary assignment of the "initial" time or GB position. For $N = l$ independent simulations of time $t = n\Delta t$, instead of defining the GB displacement $\bar{d}(i)$ from a single, fixed initial position, we redefine the GB displacement $\bar{d}(i)$ from an arbitrary position at $t = k\Delta t$ as shown in Fig. 1(b), so that

$$\bar{d}_j^k(i) = \bar{h}_j(k+i) - \bar{h}_j(k),$$

$$j = 1, 2, \ldots, l; k = 1, 2, \ldots, m; i = 1, 2, \ldots, n - m; m \le n.$$

$$(2)$$

With the new definition provided by Eq. (2), we increase the effective sample size at each GB displacement $\bar{d}(i)$ from $N = 2l$ to $N = (2l)m$. For most of the simulations in this study, we have $t = 1$ ns, $\Delta t = 1$ ps, $n = \frac{t}{\Delta t} = 1000$, $l = 12$ is the number of separate simulation runs, and we set $m = 500$ to get a good balance between the number of displacement values $\bar{d}(i)$ and the sample size for each $\bar{d}(i)$. Note that this method of statistical enhancement increases N from ~ 20 to $\sim 10^4$ for the same number of simulations, and reduces the measurement noise accordingly.

With this dramatic increase in the number of data points produced by the method, we suggest that the best way to assess the expected value $\langle \bar{d}(i) \rangle$ and variance $\langle \bar{d}^2(i) \rangle$ of each GB displacement $\bar{d}(i)$ is by fitting the $N = (2l)m$ data points to the expected distribution function, which permits finer precision than does straight averaging of the measured quantities. Specifically, to make full use of the $N = (2l)m$ data points, we fit them to a cumulative distribution function for each $\bar{d}(i)$, $i = 1, 2, \ldots, n - m$:

$$F(x) = \frac{1}{2}\left[1 + \text{erf}\left(\frac{x - \mu}{\sigma\sqrt{2}}\right)\right], \qquad (3)$$

where $F(x)$ is the probability that $\bar{d}(i)$ falls in the interval $(-\infty, x]$, erf is the error function, and $\mu = \langle \bar{d}(i) \rangle$, $\sigma^2 = \langle \bar{d}^2(i) \rangle$ are the expected value and variance of $\bar{d}(i)$. Note that Eq. (3) is the form expected based on a Gaussian distribution when it is integrated into a cumulative form.

Our adapted interface-random-walk method is validated by calculating the mobility of a Ni $\Sigma 5$ GB modeled with a Finnis-Sinclair potential [16] (referred to as Ni_{FS}) and an Al $\Sigma 7$ GB [17], as shown in Fig. 2. For comparison, results from the original interface-random-walk method of Ref. [10] are presented on the left [Figs. 2(a), 2(c), and 2(e)], and those from our adapted method are presented on the right [Figs. 2(b), 2(d), and 2(f)]. Shown in Fig. 2(a) are cumulative displacement distributions of a Ni_{FS} $\Sigma 5$ GB from $l = 12$ independent simulations when $t = 100$ ps at three temperatures; as expected the variance rises with T. Figures 2(c) and 2(e) show this increase as a function of time in both Al $\Sigma 7$ and Ni_{FS} $\Sigma 5$ GBs at different temperatures based on $l = 12$ separate simulations. There is a very high degree of scatter in these data, and it is only when the variance rises at a rate greater than the noise level that the expected linear increase is discernible; note that at 750 and 1000 K the increase is clear [Fig. 2(c)] but at 300 K it is not [Fig. 2(e)]. In fact, the result at
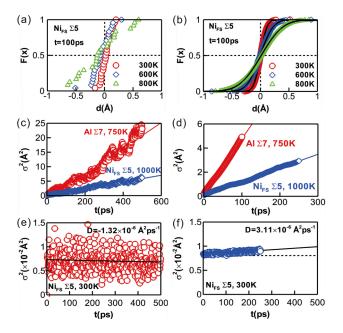

FIG. 2 (color online). Cumulative distribution of average displacement of Ni_{FS} $\Sigma 5$ GB at three temperatures when $t = 100$ ps from the (a) original and (b) adapted interface-random-walk methods; variance of the displacement of a Ni_{FS} $\Sigma 5$ GB at 1000 K and an Al $\Sigma 7$ GB at 750 K as a function of time from the (c) original and (d) adapted interface-random-walk methods; variance of the displacement of a Ni_{FS} $\Sigma 5$ GB at 300 K as a function of time from the (c) original and (d) adapted interface-random-walk methods.

750 K in Al $\Sigma 7$ ($M = 4.76 \pm 0.04 \times 10^{-7}$ m^4 J^{-1} s^{-1}) matches well with that reported in Ref. [10] ($M = 4.40 \pm 0.05 \times 10^{-7}$ m^4 J^{-1} s^{-1}) on the same GB, while the fitted slope of the data at 300 K is unphysically negative, the noise level being so high as to obscure the physics.

In contrast, consider the results obtained from the same set of simulations using the present adapted method. Figure 2(b) shows the enhanced cumulative distribution data, with $\sim 12\,000$ points determined from the very same set of simulations, which quite precisely match the expected form of Eq. (3) (marked by the black solid lines) with a coefficient of determination $R^2 = 0.9998$. With this method, at all of the temperatures presented here the variance exhibits less scatter, and therefore more subtle effects in its time evolution are revealed; note, for example, the smoother trends in Fig. 2(d) vs Fig. 2(c). Similar noise reduction is seen in Fig. 2(f) vs Fig. 2(e), and the most important result here is that the data points in Fig. 2(f) at 300 K show a clear linear dependence on time; the suppression of measurement noise in the new method allows the true physical signal to stand forth clearly. From these data the diffusion coefficient ($D = 3.11 \pm 0.14 \times 10^{-14}$ m^2 s^{-1}) and GB mobility ($M = 5.28 \pm 0.24 \times 10^{-11}$ m^4 J^{-1} s^{-1}) can be extracted at 300 K.

The reduced noise and improved resolution in our adapted implementation of the interface-random-walk method also opens the door to a new hybrid method—a biased random-walk method—that can study boundary motion under low biases and at experimentally achievable velocities. Here the migration of a Ni $\Sigma 3\{111\}$ coherent twin boundary is simulated with an EAM potential developed by Mishin et al. [18] (referred to as Ni$_{\text{Mishin}}$) at 1000 K under an artificial bias of 0.01 eV (equivalent to ~ 150 MPa in Ni) according to [8]. As shown in Fig. 3(a), the displacement distributions obtained from the adapted interface-random-walk method at $T = 1000$ K and $t = 300$ ps present only very subtle differences between the cases with and without an artificial bias. Close inspection as in the inset of Fig. 3(a) reveals a clear and measurable shift of the median GB displacement under the applied bias. The differences are even more apparent in Fig. 3(b), where the biased random walk can be tracked to extract the velocity of boundary migration (under a bias of $P = 0.01$ eV) as $v = 1.25 \times 10^{-4}$ m/s. The uncertainty on this value is $\pm 4 \times 10^{-6}$ m s^{-1}, which suggests that velocities down to perhaps a few dozen microns per second should be accessible with this method. Measurements like these are only possible because of the enhanced statistical sampling of the present method; the subtle shift in displacement statistics in Fig. 3(a) would be missed if previous methods were employed. This is shown explicitly in Fig. 3(c), where for comparison purposes the average GB position relative to a fixed starting point is presented based on a subset of 24 data points; it is difficult to tell if the GB has moved under the applied bias.

The presently measured velocity of $\sim 10^{-4}$ m/s is substantially below those reported previously using MD

simulations ($10^{-1} \sim 10^1$ m/s, [4,7–9,12–14]), and in fact lies within the range typical of experimentally measured GB velocities ($\sim 10^{-6}$ m/s to 10^{-3} m/s [1]). As an additional advantage of this hybrid technique, the variance of the distribution can still be used to assess the GB mobility as $M = 2.42 \pm 0.57 \times 10^{-13}$ m^4 J^{-1} s^{-1}, which is comparable to the value of $M = 8.50 \pm 0.27 \times 10^{-13}$ m^4 J^{-1} s^{-1} by assuming $v = MP$ [4,7–14].

As an example of the method's ability to clearly differentiate mechanistic regimes, consider Fig. 4, which is a semilog plot of GB mobility vs $1/kT$ in three different systems: Al $\Sigma 7$ and Ni $\Sigma 5$ GBs constructed from two different EAM potentials (Ni$_{\text{FS}}$ and Ni$_{\text{Mishin}}$). The temperatures range from 300 to as high as 1750 K (0.2 to $0.88T_m$) depending on the system. All of these data were acquired with our adapted interface-random-walk method, but the filled symbols in Fig. 4 specifically highlight the range of results that cannot be resolved using prior methods. It is interesting to note that in all three systems we observe two inflections separating three mechanistic regimes at low ($T < T_1 \sim 0.6T_m$), medium ($T_1 < T < T_2$), and high temperatures ($T > T_2 \sim 0.8T_m$.). The transition temperatures
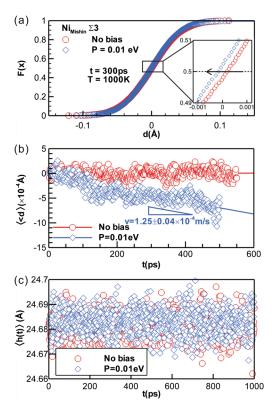

FIG. 3 (color online).   (a) Cumulative displacement distribution of a Ni$_{\text{Mishin}}$ $\Sigma 3$ coherent twin boundary at 1000 K when $t = 300$ ps with no bias and with a bias of $P = 0.01$ eV. The inset is a zoomed view of the original curves near the median. The change in average GB position with and without applied bias relative to (b) an arbitrary starting point according to Eq. (2) and (c) a fixed starting point based on 12 independent simulations.
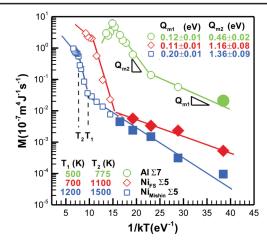
FIG. 4 (color online).   Arrhenius mobility plot for Al $\Sigma 7$, Ni_{FS} $\Sigma 5$ and Ni_{Mishin} $\Sigma 5$ GBs. The filled symbols highlight the range of results that are uniquely resolved with the present adapted method. T_1 and T_2 are transition temperatures for each system at which the slope of the fitted lines changes. Q_{m1} and Q_{m2} are activation energies in the different temperature ranges.

(T_1 and T_2) and respective activation energies (Q_{m1} and Q_{m2}) are listed in Fig. 4.

The data at medium and high temperatures in Fig. 4 mirror previously reported results using other methods. For example, the activation energies in the medium temperature range (Q_{m2} for Al $\Sigma 7$: 0.46 ± 0.02 eV, Ni_{FS} $\Sigma 5$: 1.16 ± 0.08 eV, and Ni_{Mishin} $\Sigma 5$: 1.36 ± 0.09 eV) agree very well with experimentally measured activation energies for diffusion-controlled GB migration (Al: $0.43 \sim 0.47$ eV [19] and Ni: ~ 1.18 eV [20]), which also aligns with prior simulation work that has explored the diffusion mechanism in greater detail [21,22]. Furthermore, the transition in GB motion above T_2 ($> 0.8 T_m$) can be attributed to structural transitions in the boundaries that are also well-known from prior works [4,14,23]. However, the low temperature mechanism with a low activation energy (Q_{m1}) is illuminated here owing to the adapted interface-random-walk method. This mechanism is likely related to that usually seen by MD at high boundary velocities using "driven motion" methods, which also involves a considerably lower activation energy for GB migration than that for diffusion. In those studies a mechanism of biased atomic hops across the boundary is suggested [9], and this nondiffusional mechanism is forced by virtue of the high velocities ($10^{-1} \sim 10^1$ m/s) required by the method, which swamp the slow kinetics of diffusion [16]. This mechanism has never before been observed in the zero-velocity limit, but the well-defined and extensive low temperature regime in Fig. 4 shows that this mechanism may also underlie the mobility of boundaries at low velocities and temperatures. This argument is supported by performing "driven motion" MD simulations of Ni_{FS} $\Sigma 5$ GB at 300 K following [8], from which the activation energy ($Q_{m1} = 0.125$ eV) can be extracted as the bias required to drive athermal GB motion. This value is in good agreement with that obtained in Fig. 4 ($Q_{m1} = 0.11 \pm 0.01$ eV).

In conclusion, we have adapted existing techniques to simulate GB motion such that we can now access velocities in the experimental range and extract GB mobilities at temperatures as low as $\sim 0.2 T_m$. The method reveals three mechanistic regimes of GB mobility at zero velocity. It is hoped that this method and the new regimes of behavior it can access will facilitate the unification of results from experiments and theory.

*schuh@mit.edu
[1] G. Gottstein and L. S. Shvindlerman, *Grain Boundary Migration in Metals* (CRC Press, Taylor & Francis Group, Boca Raton, 2010), 2nd ed.
[2] S. Smoluchowski, Phys. Rev. **83**, 69 (1951).
[3] C. Molteni *et al.*, Phys. Rev. Lett. **76**, 1284 (1996).
[4] B. Schönfelder *et al.*, Mater. Sci. Forum **294–296**, 9 (1999).
[5] P. Ballo and V. Slugen, Phys. Rev. B **65**, 012107 (2001).
[6] K. L. Merkle, L. J. Thompson, and F. Phillipp, Phys. Rev. Lett. **88**, 225501 (2002).
[7] H. Zhang, M. Upmanyu, and D. J. Srolovitz, Acta Mater. **53**, 79 (2005).
[8] K. G. F. Janssens *et al.*, Nature Mater. **5**, 124 (2006).
[9] H. Zhang *et al.*, Phys. Rev. B **74**, 115404 (2006).
[10] Z. T. Trautt, M. Upmanyu, and A. Karma, Science **314**, 632 (2006).
[11] S. M. Foiles and J. J. Hoyt, Acta Mater. **54**, 3351 (2006).
[12] D. L. Olmsted, S. M. Foiles, and E. A. Holm, Scr. Mater. **57**, 1161 (2007).
[13] D. L. Olmsted, E. A. Holm, and S. M. Foiles, Acta Mater. **57**, 3704 (2009).
[14] H. Zhang *et al.*, Proc. Natl. Acad. Sci. U.S.A. **106**, 7735 (2009).
[15] See supplemental material at http://link.aps.org/ supplemental/10.1103/PhysRevLett.106.045503 for geometries, potentials, and methods.
[16] G. J. Ackland *et al.*, Philos. Mag. A **56**, 735 (1987).
[17] M. I. Mendelev *et al.*, J. Mater. Res. **20**, 208 (2005).
[18] Y. Mishin *et al.*, Phys. Rev. B **59**, 3393 (1999).
[19] H. U. Schreiber and B. Grabe, Solid State Electron **24**, 1135 (1981).
[20] A. J. Detor and C. A. Schuh, J. Mater. Res. **22**, 3233 (2007).
[21] T. Kwok, P. S. Ho, and S. Yip, Phys. Rev. B **29**, 5354 (1984).**29**, 5363 (1984).
[22] V. Yamakov *et al.*, Acta Mater. **54**, 4053 (2006).
[23] D. W. Demianczuk and K. T. Aust, Acta Metall. **23**, 1149 (1975).